Synthesis of Multi-organo-functionalized Fibrous silica KCC-1 for Highly Efficient Adsorption of Acid Fuchsine and acid Orange II from Aqueous Solution

Roozbeh Soltani
Islamic Azad University, Arak
Rasool Pelalak
Islamic Azad University, Arak
Mahboubeh Pishnamazi
Islamic Azad University, Arak
Azam Marjani (azam.marjani@tdtu.edu.vn)
Islamic Azad University, Arak
Saeed Shirazian
Islamic Azad University, Arak

Research Article

Keywords: MF-KCC-1, tetrasulfide, FTIR, FESEM, EDX-Mapping, TEM

Posted Date: December 10th, 2020

DOI: https://doi.org/10.21203/rs.3.rs-122392/v1

Version of Record: A version of this preprint was published at Scientific Reports on February 1st, 2021.
See the published version at https://doi.org/10.1038/s41598-021-81080-3.

Synthesis of multi-organo-functionalized fibrous silica KCC-1 for highly efficient adsorption of acid fuchsine and acid orange II from aqueous solution

Roozbeh Soltani, Rasool Pelalak, Mahboubeh Pishnamazi, Azam Marjani*, Saeed Shirazian

Department of Chemistry, Islamic Azad University, Arak Branch, Arak, Iran

*Corresponding author; E-mail: azam.marjani@tdtu.edu.vn

Abstract

Multi-functionalized fibrous silica KCC-1 (MF-KCC-1) bearing amine, tetrasulfide, and thiol groups was synthesized *via* a post-functionalization method and fully characterized by several methods such as FTIR, FESEM, EDX-Mapping, TEM, and N_2 adsorption-desorption techniques. Due to abundant surface functional groups, accessible active adsorption sites, high surface area (572 m^2 g^{-1}), large pore volume (0.98 cm^3 g^{-1}), and unique fibrous structure, mesoporous MF-KCC-1 was used as a potential adsorbent for the uptake of acid fuchsine (AF) and acid orange II (AO) from water. Different adsorption factors such as pH of the dye solution, the amount of adsorbent, initial dye concentration, and contact time, affecting the uptake process were optimized and isotherm and kinetic studies were conducted to find the possible mechanism involved in the process. for both AF and AO dyes, the Langmuir isotherm model and the PFO kinetic model show the most agreement with the experimental data. The calculated maximum adsorption capacity for AF and AO, according to the Langmuir isotherm, was found to be 574.5 mg g^{-1} and 605.9 mg g^{-1}, respectively, surpassing most adsorption capacities reported until now which is indicative of the high potential of mesoporous MF-KCC-1 as an adsorbent for removal applications.

Introduction

Synthetic dyes are extensively used in various industries such as cosmetics, pharmaceutical, plastics, rubber, leather, textile, paper, and food, and industrial effluents containing dyes, especially in developing countries and the Third World, are mainly discharged into surface waters such as rivers, ponds, and lakes. The presence of synthetic dyes in wastewater, even at very low concentration (less than 1 mg L^{-1} in some cases), is not only aesthetically unpleasant but also causes problems for aquatic life because colored water reduces the transparency and penetration of sunlight into the water, and consequently, it disrupts the process of photosynthesis[1,2]. In addition to the negative effects mentioned above, some industrial synthetic dyes are thought to be carcinogenic, mutagenic, and teratogenic in animals and human beings[3]. For instance, acid fuchsin (AF) and acid orange II (AO) are two toxic and hazardous industrial synthetic dyes which are widely used as a corrosion inhibitor and laboratory reagent apart from their wide usage in hair dye, wool, silk, leather, nylon, and dying textile industries[4,5]. Accordingly, the removal of such

hazardous dyes from aqueous environments and waste effluents is of concern from a human health point of view.

To date, several removal methods including adsorption, ion-exchange, photocatalytic degradation, and membrane separation have been studied and used to remove synthetic dyes from aqueous environments. Among them, the adsorption technique has attracted a great deal of attention because it is a more efficient, simple, versatile, cost-effective, and best-suited process for the removal of synthetic dyes like AF and AO[6–9].

A vast variety of materials, including mesoporous silica materials (MSMs)[8,10], metal-organic frameworks and their composites[6,11], covalent organic frameworks and their composites[12,13], graphene and graphene oxide-based materials[14,15], etc. are utilized as adsorbents to remove organic synthetic dyes from aqueous media and wastewater. Among those adsorbents, MSMs-based adsorbents have shown excellent performance due to their environment-friendly water-based synthesis methods (sol-gel process), porous structure, large surface area, high pore volume, designable structure and morphology, functionalizable surface, good chemical and thermal stability, and reusability[7,8,10,16]. Although pure silicas are inherently able to adsorb organic synthetic dyes due to their large number of surface silanol groups (through hydrogen bonding), it is believed that the surface functionalization process is an indispensable operation for increasing the absorption performance of these materials[10,17,18]. For this purpose, one of the best options available for surface functionalization is the use of silane coupling agents (SCAs), which in addition to establishing a strong covalent bond with surface silanol groups possess a high diversity of organic functional groups bearing oxygen, nitrogen, and sulfur atoms.

One of the newest members of the MSMs family is fibrous silica KCC-1, which was first synthesized and characterized in 2010 by Polshettiwar et al[19]. Unlike conventional ordered MSMs such as FDU-12, KIT-6, KIT-5, SBA-16, SBA-15, MCM-48, MCM-41, etc., in which the large surface area is related to their regular pore structure, in KCC-1, the high surface area is due to the presence of regular and concentric fibers that have grown radially from the center of the silica spheres to the outside of the sphere[20]. It has been reported that due to this unique feature easier access to the surface silanols of these fibers is possible because unlike ordered MSMs, the pore-blocking phenomenon does not occur during the surface modification or synthesis process which makes them inaccessible[21–24]. Therefore, KCC-1 can be a suitable candidate for adsorption and

catalysis applications where the need for high surface area and accessible active sites is the first priority. In the application of adsorption, this material can especially play the role of adsorbent *via* functionalization of its surface with a wide variety of functional groups as potential adsorption sites.

In this research work, a multi-functionalized KCC-1 (MF-KCC-1) bearing amine ($–NH_2$), thiol (–SH), and tetrasulfide (–S–S–S–S–) groups was synthesized *via* a post-modification (or post-functionalization) method and used as a potential adsorbent for removal of AF and AO dyes from water. The impact of important adsorption factors, including pH, the amount of adsorbent, initial dye concentration, and contact time, on the adsorption procedure were studied and optimal adsorption conditions were found. To find possible absorption mechanisms involved in the removal process, isotherm and kinetic studies were conducted and the corresponding absorption parameters were investigated and compared. The adsorption performance of MF-KCC-1 was compared with previous adsorbents toward AF and AO.

Results and discussion

Synthesis of KCC-1 and MF-KCC-1. Mesoporous KCC-1 was synthesized via a conventional sol-gel-hydrothermal method in a stainless-steel autoclave. In this synthesis process, TEOS, CTAB, n-amyl alcohol, cyclohexane, and Urea was used as silica source, structure-directing agent (template), co-surfactant (for stabilizing the micelles/microemulsion droplets), co-solvent, and hydrolyzing agent, respectively. Due to the presence of many silanol groups on the surface of silica fibers of KCC-1, SCAs can be easily attached to them and cover the entire length of the fibers by establishing strong chemical bonds as shown in Figure 1. Unlike common ordered MSMs which are prone to pore blocking phenomenon (this practically leads to the inaccessibility of a number of adsorption sites inside the pores and channels), MF-KCC-1 is able to provide more available adsorption sites to adsorbed species due to its unique fibrous structure. Also, in comparison with MF-KCC-1, the continuous channel structure in ordered MSMs limits the rate of penetration of adsorbates into these channels and reaching adsorption sites. Therefore, it seems that the fibrous structure of KCC-1 with its high accessible surface area can be a good platform for surface functionalization and use to adsorb species.

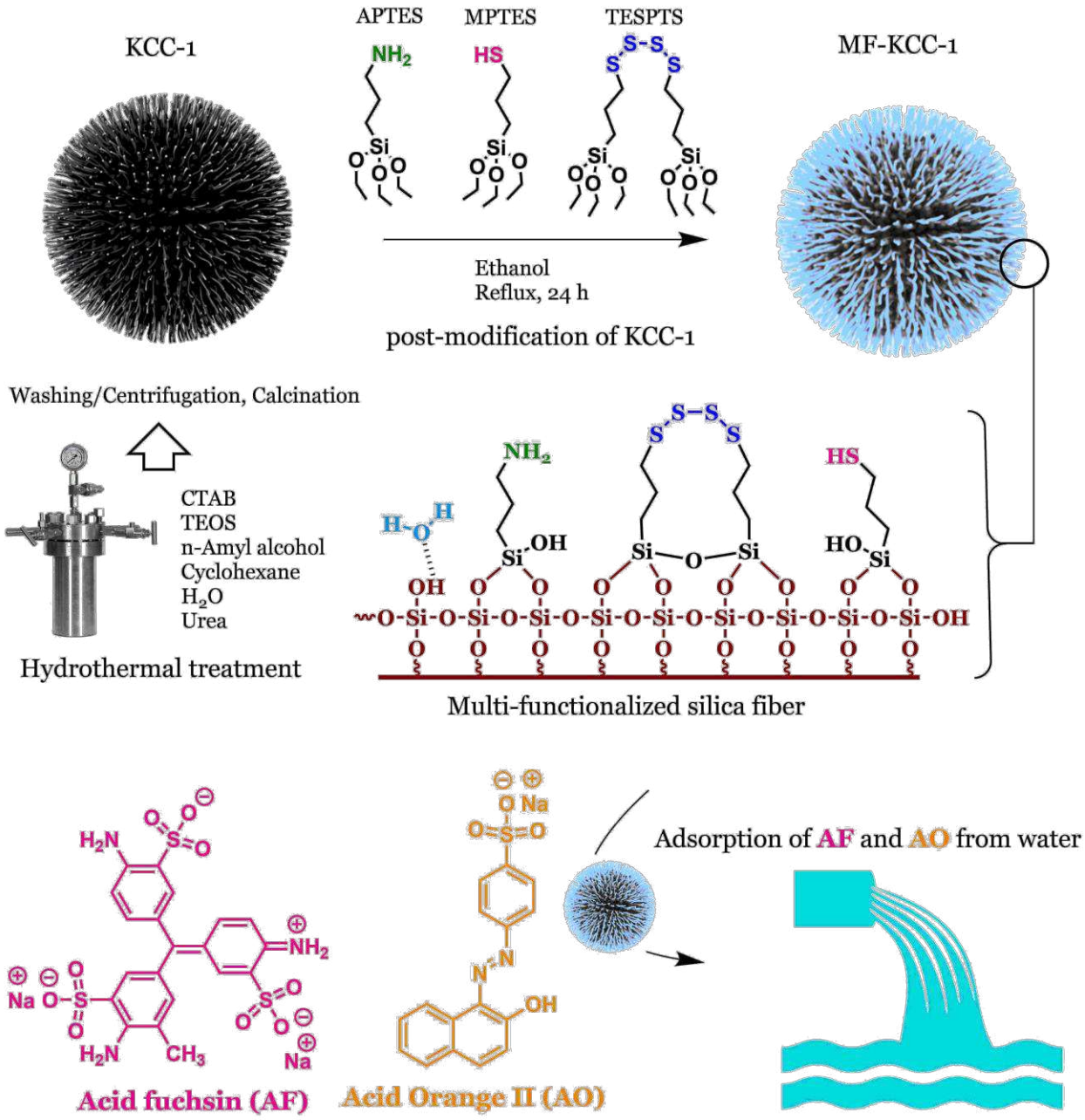

111

112 **Figure 1.** The overall process of synthesizing KCC-1 and MF-KCC-1 and molecular structure of AF and AO dyes.

113 ## Characterization of the KCC-1 and MF-KCC-1

114 **FTIR analysis.** FTIR spectra of KCC-1 and MF-KCC-1 are shown in Fig. 2. In the case of KCC-
115 1, the characteristic absorption bands at 465 cm^{-1}, 808 cm^{-1}, 965 cm^{-1}, and 1095 cm^{-1} are observed
116 which are attributed to the bending vibration of Si–O–Si, Si –O stretching vibrations, Si–OH
117 stretching vibrations, and Si–O–Si stretching vibrations, respectively. The FTIR band at 1640 cm^{-}

[1] is due to the bending mode of surface adsorbed water molecules. The broad absorption band centered at 3434 cm^{-1} is assigned to the stretching vibrations of SiO–H groups (silanols) as well as surface adsorbed water. The incorporation of SCAs containing $–NH_2$, –SH, and –S–S–S–S– groups in the silica frameworks of KCC-1 can be qualitatively confirmed by the FTIR spectrum shown in Fig. 2. At 560-680 cm^{-1} two weak absorption bands are seen which are due to –S–S–S–S– stretching vibrations, and C–S stretching mode at 690 cm^{-1}, indicating the existence of tetrasulfide groups as well as thiol groups. FTIR band at 1470 cm^{-1} is assigned to the bending vibration of $–CH_2–$ groups in the SCAs structure. The weak absorption band at 5575 cm^{-1} is attributed to the S–H stretching vibration. Two characteristics absorption bands at 2870 cm^{-1} and 2940 cm^{-1} are related to the symmetric and asymmetric C–H stretching vibrations. Broad absorption band between 3600-3100 cm^{-1} is due to the presence of amine and hydroxyl (silanols) groups and two bands around 3355 cm^{-1} are attributed to the symmetric and asymmetric N–H stretching vibrations.

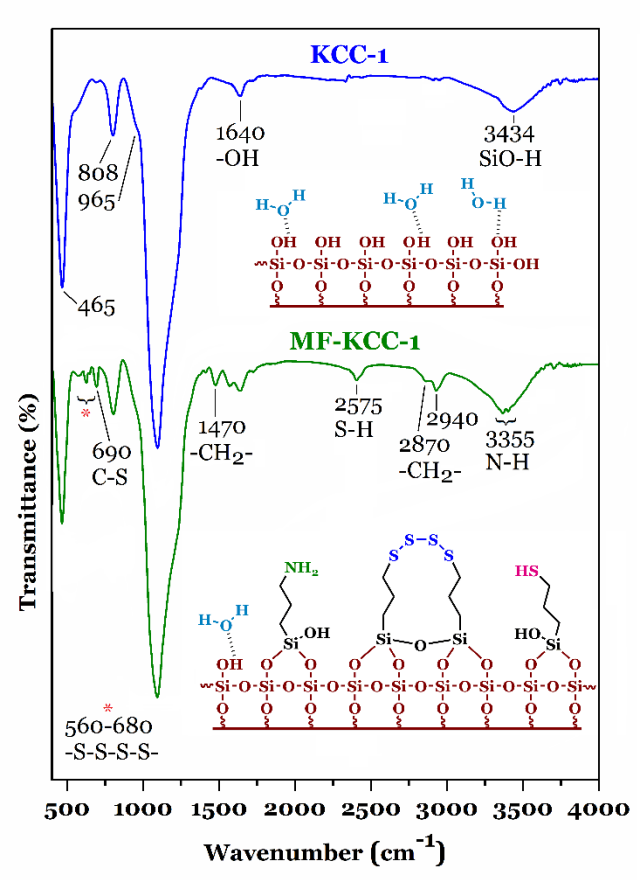

Figure 2. FTIR spectra of the samples.

Theses above-mentioned results indicate the successful grafting of SCAs on the KCC-1 surface and are in good agreement with previous reports concerning the synthesis of silica frameworks and grafting of SCAs on nanoporous silica materials[7,10,25–27].

FESEM, TEM, and EDX dot mapping analyses. The surface morphology of the samples (Fig. 3), fibrous structure of silica spheres (Fig. 4), and distribution of elements on the surface of the MF-KCC-1 (Fog. 4) were observed by FESEM, TEM, and EDX mapping images.

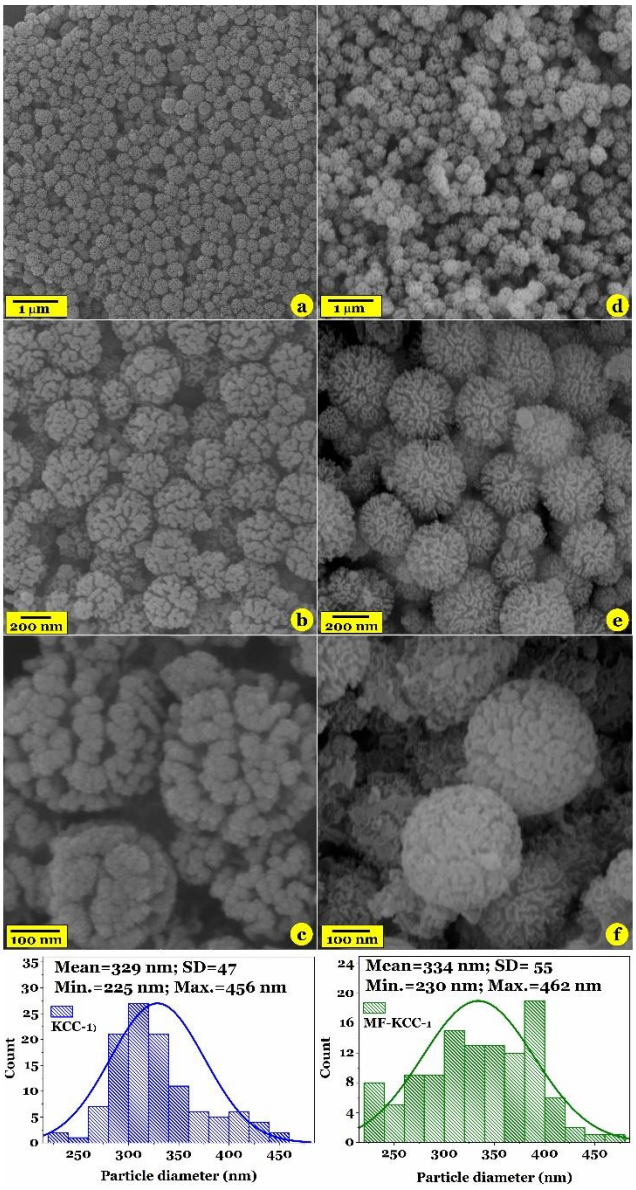

Figure 3. FESEM images of pure KCC-1 (a-c) and MF-KCC-1 (d-f) and corresponding particle size histograms.

142

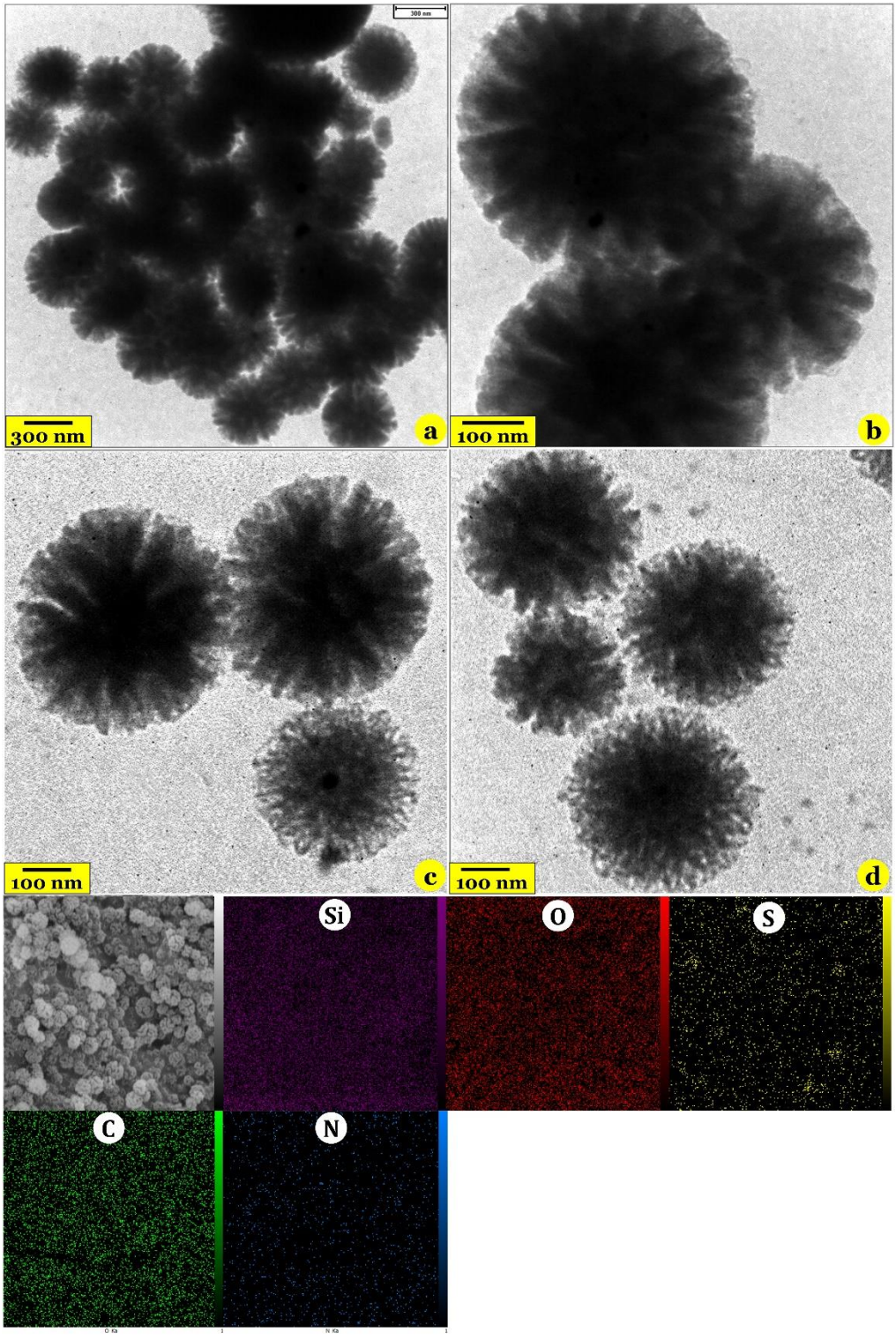

143

144 **Figure 4.** TEM images of the pure KCC-1 (a and b) and MF-KCC-1 (c and d) and EDX dot elemental mapping images
145 of the MF-KCC-1 (the third and fourth rows).

Consistent with previous reports, FSEM images of both KCC-1 (Fig. 3a-c) and MF-KCC-1 (Fig. 3d-f) reveal that these materials consist of colloidal spheres of uniform size with wrinkled morphology. The particle-size histograms of samples showed that the diameter of KCC-1 and MF-KCC-1 range from 225 nm to 456 nm and from 230 nm to 462 nm, respectively. The slight increase in the size of the spheres after surface modification is probably due to the chemically grafting of SCAs on the KCC-1 particles. Comparing the FESEM images of the samples, it seems that the thickness of the wrinkled layers of silica spheres has decreased after surface functionalization, which is probably due to the repulsion between the organic chains of SCAs as well as the ultrasonication process. Close inspection of these samples by TEM technique indicate that both KCC-1 and MF-KCC-1 have dendrimeric fibers arranged in 3D space to form uniform spheres (Figure 4). However, by comparing the TEM images of the samples, it can be seen that the density of fibers in the pure KCC-1 (Figs. 4a and b) is higher than that of the MF-KCC-1 (Figs. 4c and d) which is due to the repulsion between silica fibers coated with SCAs as mentioned above. Similar observations have been reported by Soltani and his colleagues[8,22,23]. The elemental composition of the MF-KCC-1 was abstained from EDX mapping analysis and presented in Fig. 4 and reveals that MF-KCC-1 contains Si, S, O, N, and C elements which are homogeneously distributed on the surface of fibrous spheres.

Surface area, pore volume, and pore diameter measurements. The N_2 adsorption-desorption isotherms of KCC-1 and MF-KCC-a revealed characteristic type IV curve with typical H3 hysteresis loop (Fig. 5), which is consistent with literature reports on standard KCC-1[20,28]. As for pure KCC-1, the Brunauer–Emmett–Teller (BET) surface area, Langmuir, surface area, total pore volume (TPV), and Barrett–Joyner–Halenda (BJH) average pore diameter are obtained as 725 m^2 g^{-1}, 751 m^2 g^{-1}, 1.35 cm^3 g^{-1}, and 3.52 nm respectively, whereas the corresponding parameters of MF-KCC-1 have decreased to 572 m^2 g^{-1}, 603 m^2 g^{-1}, 0.98 cm^3 g^{-1}, and 2.23 nm as shown in Table 1. This reduction in surface area, pore volume, and pore size during the surface functionalization process with SCAs is an expected phenomenon due to the introduction of organic content into the pore structure. However, even after surface functionalization, MF-KCC-1 possesses a large surface area high pore volume that can make it a potential material for use in adsorption and catalyst applications.

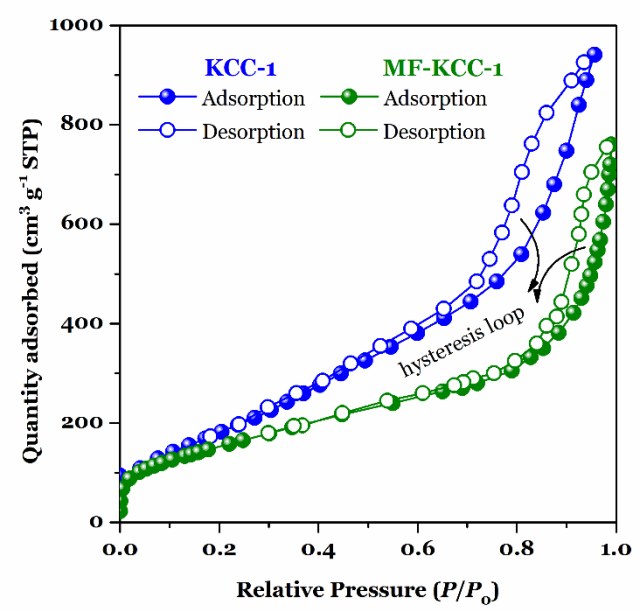

Figure 5. The N_2 adsorption-desorption isotherms of KCC-1 and MF-KCC-1.

Table 1. Textural properties of KCC-1 and MF-KCC-1.

Samples	S_{BET} (m^2 g^{-1})	$S_{Langmuir}$ (m^2 g^{-1})	TPV (cm^3 g^{-1})	APD (nm)
KCC-1	725	751	1.35	3.52
MF-KCC-1	572	618	0.98	2.23

Adsorption studies

The impact of pH and adsorbent dosage. The simultaneous effect of adsorbent dosage and pH on the adsorption of AF and AO was investigated. According to the adsorption data given in Fig. 6, as the amount of adsorbent increases from 0.033 g L^{-1} to 0.100 g L^{-1}, the removal percentage increases continuously for both AF and AO dyes. With further increase in the adsorbent dosage, the removal percentage does not show a significant increase. Therefore, it can be concluded that, for both AF and AO dyes, at a concentration of 10 mg L^{-1} and an adsorbent dosage of 0.100 g L^{-1} almost all absorption sites are saturated. Also, for both AF and AO days, the highest removal percentages were observed at pH 3.0 to 4.0 in all absorbent dosages. For AF and AO adsorption, the maximum uptake occurred at pH 3.0 and was up to 93.5% and 99.5%, respectively. As the pH of the solution increases, the removal percentage decreases steadily until at pH=8.0 the removal

percentages of AF and AO decrease to 55% and 66%, respectively. A similar trend has been reported in previous studies concerning adsorption of AF and AO by silica-based adsorbents[1,29]. At low pH, the surface of MF-KCC-1 became positively charged because of the protonation of functional groups. The positively charged surface of the MF-KCC-1 captures negatively charged anionic AF and AO dyes in an aqueous medium through electrostatic attraction. As the pH of the solution augments, the surface charge density starts to decrease and the hydroxide ion concentration increases simultaneously, resulting in a decrease in adsorption of dyes by the adsorbent according to the following two main mechanisms[8]:

1) a decrease in the attractive electrostatic interactions between the surface of MF-KCC-1 and the anionic dye molecules due to electrostatic repulsion between the negatively charged surface of the adsorbent and anionic dyes.
2) The competitive behavior between hydroxide ions and anionic molecules for available adsorption sites.

Accordingly, the adsorbent dosage of 0.100 g L^{-1} and pH=3.0 were chosen as optimal adsorbent dosage and solution pH for further investigations.

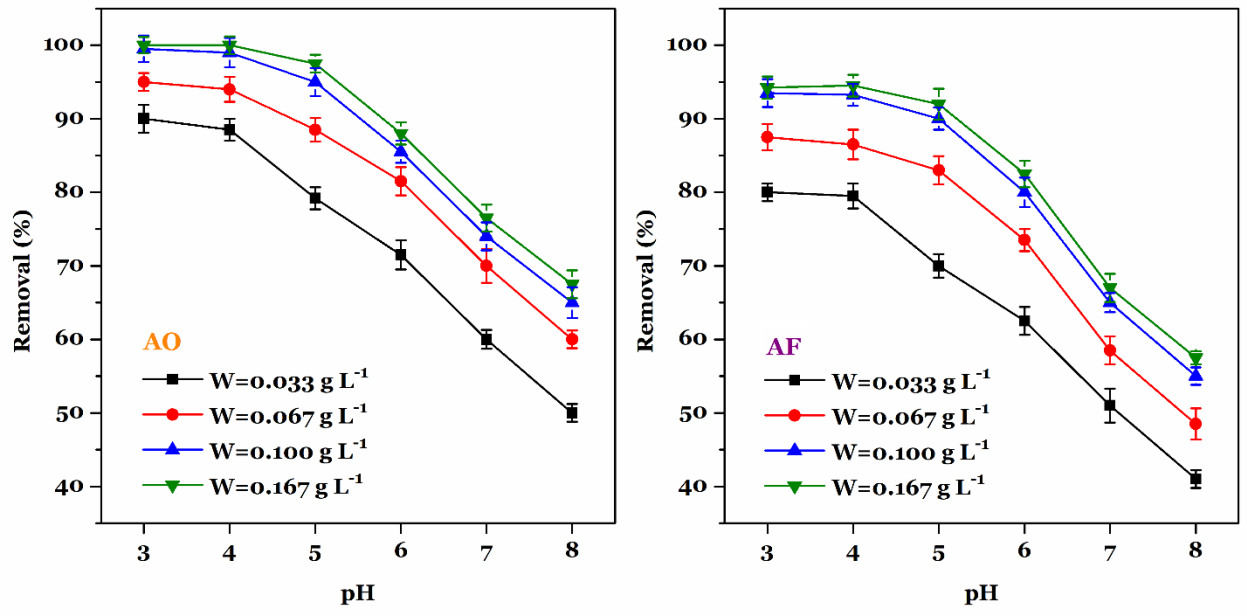

Figure 6. The effect of pH and adsorbent dosage on the removal percentage of AF (left) and AO (right) dyes (C_i=10 mg L^{-1}, t=120 min, T=25 °C, shaking speed =180 rpm).

The impact of initial dye concentration and isotherm studies. The effect of initial concentration on the adsorption capacity of AF and AO were studied and different nonlinear isotherm models, namely Langmuir (Eq. 4, Table 2), Freundlich (Eq. 5, Table 2), and Redlich-Peterson (R-P, Eq. 6, Table 2), were used to fit the experimental data. As shown in Fig. 7a and b, for both AF and AO dyes, with augmenting the concentration the adsorption capacity increases continually.

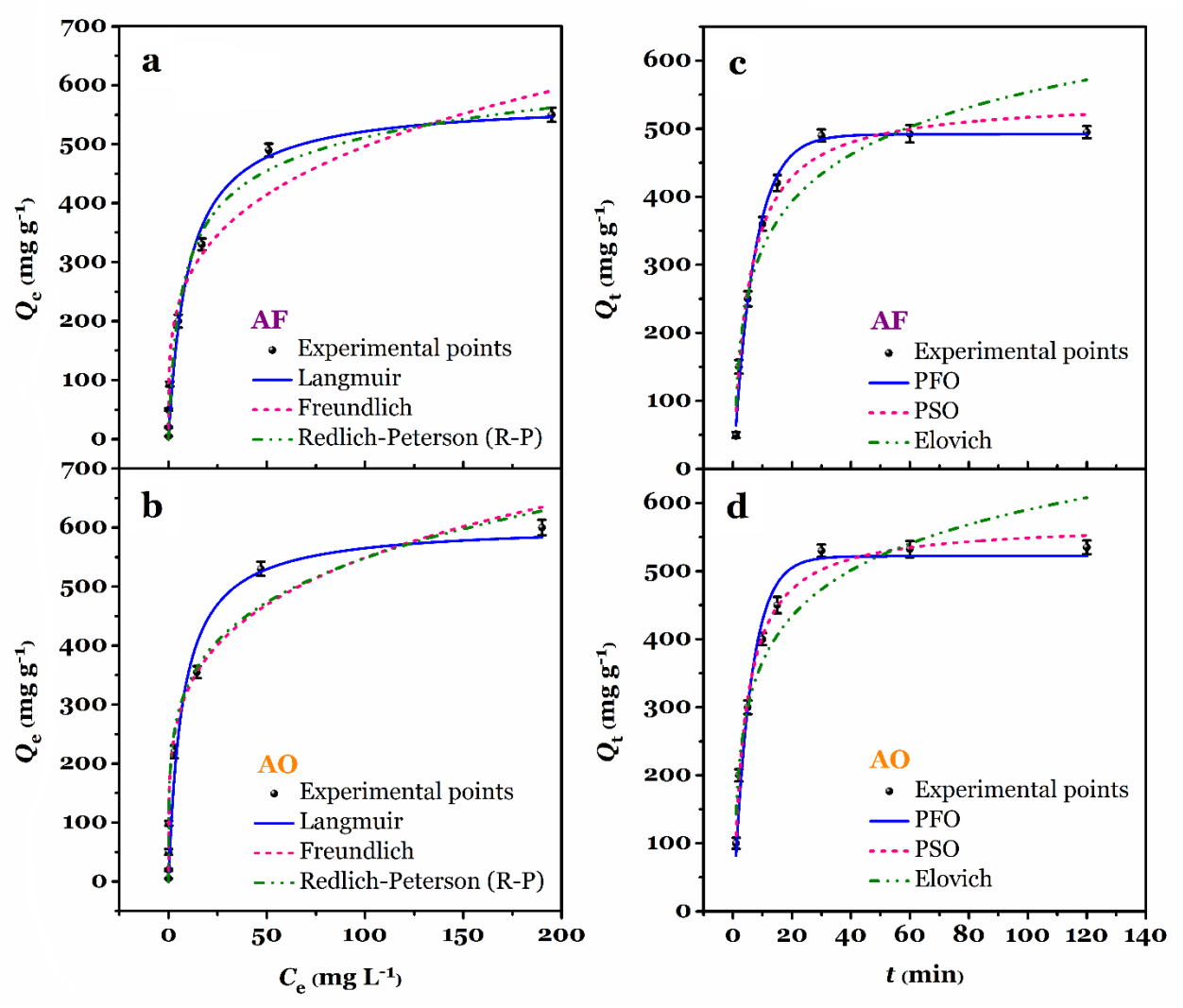

Figure 7. The effect of initial dye concentration on the adsorption capacity of AF (a) and AO (b) dyes and corresponding isotherm curves (pH=3.0, W= 0.100 g L^{-1}, C_i=0.5-250 mg L^{-1}, t=120 min, T=25 °C, shaking speed=180 rpm). The effect of time on the adsorption capacity of AF (a) and AO (b) dyes and corresponding kinetic curves (pH=3.0, W= 0.100 g L^{-1}, C_i=100 mg L^{-1}, t=1-120 min, T=25 °C, shaking speed=180 rpm).

However, in the initial concentrations of 0.5 to 100 mg L^{-1}, the adsorption capacity increases with a sharp slope, but at concentrations above 100 mg L^{-1}, the adsorption slope decreases until it reaches an almost constant value at an initial concentration of 250 mg L^{-1}. The maximum experimental adsorption capacity ($Q_{m,exp.}$) for AF and AO were 550.5 and 600.0 mg g^{-1}, respectively.

To better understand the adsorption isotherms involved in the removal process of AF and AO by MF-KCC-1 from aqueous media, Langmuir, Freundlich, and R-P isotherm models were used and the relevant parameters after nonlinear regression analysis were given in Table 2.

For AF adsorption, the obtained R^2 values, after nonlinear fitting of isotherm models, are in the following order: 0.9731 for Langmuir, 0.9713 for R-P, and 0.9547 for Freundlich. For AO adsorption, the R^2 values are in the following order: 0.9707 for Freundlich, 0.9672 for R-P, and 0.9527 for Langmuir. Although the R^2 values obtained for both Langmuir and Freundlich models are high, other isotherm parameters must be considered to determine which model is more consistent with the experimental data.

As tabulated in Table 2, for both AF and AO, the calculated maximum adsorption capacity ($Q_{m,cal.}$=574.5 mg g^{-1} for AF and $Q_{m,cal.}$=605.9 mg g^{-1} for AO) obtained by the Langmuir model is close to the corresponding experimental value ($Q_{m,exp.}$=550.5 mg g^{-1} for AF and $Q_{m,exp.}$=600.0 mg g^{-1} for AO), indicating the good agreement of this model with the experimental data. Also, according to the literature review, the closer the g parameter in the R-P equation is to one and zero, the closer the experimental data are to the behavior of the Langmuir and Freundlich isotherms, respectively (for g=1 and g=0 the R-P model becomes the Langmuir and the Freundlich model)[13,22,25]. The obtained g values for adsorption of AF and AO were found to be 0.8978 and 0.7893 which is indicative of a closer correlation of the adsorption isotherm data of both dyes with the Langmuir model.

Based on the Langmuir model, it can be assumed that AF and AO anionic molecules adsorb on a monomolecular layer of the MF-KCC-1 with unique localized adsorption sites without any special interaction between these dye molecules.

Table 2. Nonlinear forms of isotherms and kinetics equations and corresponding parameters and values.

	Models	Equations	Parameters[a]	Values AO	AF
	Isotherms		$Q_{m,exp.}$(mg g^{-1})	600.0	550.5
(4)	Langmuir	$Q_e = \frac{Q_{m,cal.} \cdot K_L \cdot t}{1 + K_L \cdot C_e}$	$Q_{m,cal.}$(mg g^{-1})	605.9	574.5
			K_L(L mg^{-1})	0.1388	0.0991
			R^2	0.9527	0.9731
(5)	Freundlich	$Q_e = K_F \cdot C_e^{1/n}$	K_F((mg g^{-1}) (L mg^{-1})$^{1/n}$)	193.8	149.7
			n(–)	4.422	3.841
			R^2	0.9707	0.9547
(6)	R-P	$Q_e = \frac{K_{RP} \cdot C_e}{1 + \alpha_{RP} \cdot C_e^g}$	K_{RP}(L g^{-1})	3210.2	92.58
			α_{RP}(mg L^{-1})$^{-g}$	15.409	0.2734
			g ($0 < g < 1$)	0.7893	0.8978
			R^2	0.9672	0.9713
	Kinetics		$Q_{e,exp.}$(mg g^{-1})	535.2	495.1
(7)	PFO	$Q_t = Q_{e,cal.} \cdot (1 - e^{-k_1 \cdot t})$	$Q_{e,cal.}$(mg g^{-1})	521.8	491.8
			k_1(min^{-1})	0.1711	0.1394
			R^2	0.9704	0.9921
(8)	PSO	$Q_e = \frac{Q_{e,cal.}^2 \cdot k_2 \cdot t}{1 + Q_{e,cal.} \cdot k_2 \cdot t}$	$Q_{e,cal.}$(mg g^{-1})	571.5	544.5
			$k_2 \times 10^{-4}$(g mg^{-1} min^{-1})	4.22	3.41
			R^2	0.9904	0.9801
(9)	Elovich	$Q_t = \frac{1}{\beta} \cdot \ln(\alpha \cdot \beta) \cdot t$	α(mg g^{-1} min^{-1})	424.1	255.4
			$\beta \times 10^2$(g mg^{-1})	1.03	1.01
			R^2	0.9174	0.9103

[a] $Q_{m,exp.}$: experimental maximum adsorption capacity; $Q_{m,cal.}$: calculated maximum adsorption capacity; K_L: Langmuir isotherm constant; K_F: Freundlich isotherm constant; n: Freundlich isotherm constant; K_{RP} and α_{RP} are R-P isotherm constant; g is R-P isotherm constant; $Q_{e,exp.}$: experimental adsorption capacity at equilibrium; $Q_{e,cal.}$: calculated adsorption capacity; k_1: PFO rate constant; k_2: PSO rate constant; α and β are Elovich kinetic consatnts.

The impact of contact time and kinetic studies. The impact of contact time in the adsorption process is of great economic importance. Accordingly, the effect of contact time on the adsorption of AF and AO MF-KCC-1 was monitored and the obtained results are given in Fig. 7c and d. The amount of absorption capacity for both AF and AO reached its maximum in the first 30 min and then reaches equilibrium. Consequently, in the removal process of AF and AO, 30 min contact time is the optimal time to reach adsorption equilibrium. In order to investigate the adsorption mechanisms involved in the adsorption process of AF and AO by MF-KCC-1, three different kinetic adsorption models, including pseudo-first-order (PFO), pseudo-first-order (PSO), and Elovich, were used, and corresponding computational data and R^2 values after nonlinear fitting are given in Table 2. According to the data in Table 2, the PFO and PSO kinetic models have a

higher R^2 values than the Elovich kinetic model, which indicates that PFO and PSO models are better consistent with the experimental adsorption data. The R^2 trend for kinetic models is as follows: for adsorption of AF: PFO (R^2=0.9921)>PSO (R^2=0.9801)>Elovich (R^2=0.9103); and for adsorption of AO: PSO (R^2=0.9904)>PFO (R^2=0.9704)> Elovich (R^2=0.9174). Comparing the R^2 values for the PFO and PSO models, it is clear that the PFO and PSO models have higher R^2 values for AF and AO, respectively. However, for the adsorption of both dyes, the equilibrium adsorption capacities ($Q_{e,exp.}$=$Q_{e,exp.}$=495.1 mg g^{-1} for AF and 535.2 mg g^{-1} for AO) are more in line with the theoretical adsorption capacities ($Q_{e,cal.}$=491.8 mg g^{-1} for AF and $Q_{e,cal.}$=521.8 mg g^{-1} for AO) obtained from the PFO model, indicating that the PFO model is more consistent with the experimental data than the PSO model. As a result, the adsorption kinetics of AF and AO are a combination of both PFO and PSO kinetic models, in which the PFO kinetic model (fast adsorption response) plays a more significant role.

Comparison study. The MF-KCC-1 showed a remarkable adsorption performance for both AF and AO compared with other adsorbents both in terms of adsorption capacity and in terms of adsorption time. According to Table 3, only the adsorbent prepared by Soltani et al. (LDH/MOF HNC, 2020)[6] shows both higher adsorption capacity and shorter adsorption time compared to MF-KCC-1 adsorbent, and the other adsorbents show lower adsorption performance than MF-KCC-1.

Table 3. Maximum adsorption capacities for AF and AO by various adsorbents (NR: not reported; DDW: double distilled water; RT: room temperature)[a].

		$Q_{m,cal.}$ (mg g^{-1})		Conditions			
Adsorbents	Year	AO	AF	pH	t (min)	T (°C)	Ref.
MF-KCC-1	2020	605.9	574.5	3.0	30	25	This work
NH_2-MIL-101(Cr)@Au	2020	419.85	-	5.0	30	RT	[30]
LDH/MOF HNC	2020	1173	-	7.0	15	20	[6]
de-oiled biomass	2019	-	9.9	DDW	50	35	[5]
γ-Fe_2O_3@C@UiO-66-NH_2	2019	48.12	31.54	NR	180	25	[31]
CMC/BC	2018	-	253.2	2.0	60	20	[32]
MnO_2/MCM-41	2015	909.99	716.17	2.0	150	20	[1]
HCZ	2014	38.96	-	1.0	60	30	[33]
NH_2-MCM-41	2014	278.38	140.60	2.0-3.0	240	25	[29]
CMC	2013	-	105.71	5.0	120	25	[34]

[a] Biomass: *Sargassum myriocystum*; CMC/BC: carboxymethyl-chitosan/bentonite composite; CMC: chemically modified cellulose; HCZ: hexadecyltrimethylammonium bromide coated zeolite.

This excellent adsorption performance may be owing to the unique fibrous structure of the MF-KCC-1 which facilitates easier access to abundant surface adsorption sites. Also, many functional organic groups like –SH, –S–S–S–S–, and $–NH_2$ grafted on the surface of silica fibers increase attractive interactions with the AF and AO dye molecules.

Conclusion

In summary, we have synthesized a multi-functionalized fibrous silica KCC-1 bearing amine ($–NH_2$), mercapto (–SH), and tetrasulfide (–S–S–S–S–) functional groups. Pure KCC-1 was prepared based on a conventional sol-gel-hydrothermal method and then functionalized *via* a simple post-grafting approach to yield MF-KCC-1. FESEM and TEM images revealed that both KCC-1 and MF-KCC-1 particles possess a wrinkled spherical morphology and uniform fibrous structure, respectively. BET model revealed that KCC-1 and MF-KCC-1 have a high surface area of 725 m^2 g^{-1} and 572 m^2 g^{-1}, respectively, with mesoporous structure. Due to its high surface area, abundant active surface groups, and unique fibrous structure, MF-KCC-1 was used as an adsorbent to remove AF and AO anionic dyes from aqueous media. The impact of important adsorption factors, such as pH, adsorbent dosage, initial dye concentration, and contact time, on the removal process were investigated and optimal conditions were obtained. To gain a better understanding of plausible adsorption mechanisms involved in the adsorption process, isotherm and kinetic studies were conducted and it was found that among the different isotherm and kinetic models used for both AF and AO dyes the Langmuir isotherm model and the PFO kinetic model show the most agreement with the experimental data. The calculated maximum adsorption capacity for AF and AO, according to the Langmuir model, was found to be 574.5 mg g^{-1} and 605.9 mg g^{-1}, respectively, surpassing most adsorption capacities reported until now. We believed that the described fabrication method and adsorbent design in this study can inspire the synthesis and development of new multi-functionalized KCC-1 nanoparticles for use as adsorbents in environmental applications like adsorption, extraction, and even catalysis.

Material and methods

Chemicals. Tetraethyl orthosilicate (TEOS, ≥99%), cetyltrimethylammonium bromide (CTAB, ≥99%), (3-aminopropyl)triethoxysilane (APTES, 99%), bis[3-(triethoxysilyl)propyl] tetrasulfide

(TESPTS, ≥90%), (3-mercaptopropyl)triethoxysilane (MPTES, ≥80%), acid Fuchsin (AF, dye content 70%), acid orange II (AO, ≥98%) were purchased from Sigma-Aldrich (Germany). Cyclohexane (≥99.9 %), hydrochloric acid (HCl, 37%), urea (≥99%), n-amyl alcohol (≥98.5), and sodium hydroxide (NaOH, pellets, ≥97%) were purchased from Merck Millipore (Germany). Ethanol (96% and absolute) and acetone (HPLC grade) were purchased from Mojallali Chemical Co. (Tehran, Iran).

Synthesis of KCC-1 and MF-KCC-1. Pure KCC-1 was fabricated according to a typical sol-gel-hydrothermal method (in an Teflon-lined stainless steel autoclave) reported by Soltani et al[8,23]. In a typical synthesis route, in a 1-L Teflon cylinder, urea (3.6 g, 59.9 mmol) and CTAB (3 g, 8.23 mmol) were first dissolved in 250 mL pure water under stirring for 15 min at 25 ℃. To the above solution, a mixture of TEOS (15 mL, 72 mmol) and cyclohexane (250 mL) was added. The mixture was further stirred for 15 min and then n-amyl alcohol (18 mL) was added. The mixture was stirred for 20 min before placing the Teflon container in a stainless-steel autoclave. The autoclave was then transferred to an electric oven and kept at 120 ° C for 6 h. At the end of the reaction, the autoclave was allowed to cool to room temperature. The white gel-like product was separated by centrifugation and washed several times with ethanol and water, followed by oven-drying (60 °C, overnight) and calcination (550 °C, 6 h) in the air to yield fine white powders of pure KCC-1.

KCC-1 was functionalized with SCAs, namely APTES, MPTES, and TESPTS, *via* the following post-modification technique. In a typical procedure, 3 g KCC-1 and 300 mL ethanol were added into a 1-L round bottom flask and ultrasonicated for 15 min. Afterward, 1.5 mL of SCAs mixture (molar ratio APTES/MPTES/TESPTS=1:1:1) was added to the flask and ultrasonicated for a further 15 min, followed by refluxing for 24 h. After cooling to room temperature, the obtained white product was centrifuged, rinsed repeatedly with ethanol and water, and oven-dried (60 °C for 24 h) to yield MF-KCC-1.

Instruments and characterization of samples. In order to investigate the qualitative characterization of functional groups of samples and also to find out whether SCAs had been grafted on KCC-1 successfully, Fourier Transform Infrared (FTIR, Avatar 370, Thermo Nicolet, USA) spectra of the samples were recorded from 4000-400 cm^{-1} wavenumber.

A Field emission scanning electron microscope (FE-SEM, MIRA3 TESCAN-XMU, Kohoutovice, Czech Republic) was applied to observe the surface morphology of KCC-1 and MF-KCC-1 before and after grafting of SCAs on the surface of KCC-1. An energy-dispersive X-ray (EDX) spectrometer was used so as to observe the distribution of the elements on the surface of KCC-1.

The fibrous structure of the samples was visualized by a Transmission electron microscope (TEM, Philips CM120) with a tension voltage of 120 kV.

To measure the porosity and adsorption behavior of the KCC-1 and MF-KCC-1, a volumetric N_2 adsorption-desorption apparatus (BELSORP-mini II, Osaka, Japan) was used. The surface area of the samples was calculated according to the Brunauer-Emmett-Teller (BET) and Langmuir models. the Barrett–Joyner–Halenda (BJH) method was used to measure the pore volume and pore sized distribution of the samples.

The concentrations of AF and AO in the aqueous solutions were measured using a Spectrophotometer (Model, UV-1201, Shimadzu, Tokyo, Japan) at $\lambda_{max.}$=524 nm and λ_{max}=486 nm, respectively.

Adsorption experiments. The removal percentage and adsorption capacities at equilibrium (Q_e, mg g^{-1}) and any time t (Q_t, mg g^{-1}) were calculated using the following equations:

$$\%Remival = \frac{C_i - C_e}{C_i} \times 100 \qquad (1)$$

$$Q_e = (C_i - C_e) \times \frac{V}{W} \qquad (2)$$

$$Q_t = (C_i - C_t) \times \frac{V}{W} \qquad (3)$$

where, C_i (mg L^{-1}), C_e (mg L^{-1}), and C_t (mg L^{-1}) are initial concentration, equilibrium concentration, and concentration at any time t, respectively. V (mL) and W (g L^{-1}) represent the volume of solution and the amount of adsorbent, respectively.

The simultaneous effect of pH and adsorbent dosage (W, g L^{-1}) was investigated by adding a certain amount of MF-KCC-1 (W= 0.033, 0.067, 0.100, and 0.167 g L^{-1}) into 100-mL polypropylene bottles containing 30 mL AF and AO severally. The bottles were shacked using an

IKA KS 3000ic control incubator shaker (Germany) at 180 rpm min^{-1} for 120 min at 25℃. Initial concentrations of both dyes were 10 mg L^{-1}. After shaking, the samples were centrifuged and the residual concentrations of each dye in the solutions were measured by UV spectrophotometer.

Moreover, the impact of the initial concentration of dye on the adsorption performance was investigated by the same procedure and diluting stock solutions (1000 mg L^{-1}) of AF and AO into 0.5, 2, 5, 10, 25, 50, 100, and 250 mg L^{-1} (pH=3.0, V=30 mL, W=0.100 g L^{-1}, t=120 min, T=25 ℃, shaking speed=180 rpm min^{-1}). In a similar way, the effect of contact time on the adsorption was conducted by measuring the concentration of samples at 1, 2, 5, 10, 15, 30, 60, and 120 min contact time (C_i=100 mg L^{-1}, pH=3.0, V=30 mL, W=0.100 g L^{-1}, T=25 ℃, shaking speed=180 rpm min^{-1}).

Author contributions

Roozbeh Soltani conceived the idea of preparing MF-KCC-1 material, designed the study on the synthesis of MF-KCC-1 material, synthesized and characterized KCC-1 and MF-KCC-1, conducted the adsorption studies, computed the theoretical adsorption data, analyzed the results, supervised the project, and wrote and edited the paper. **Rasool Pelalak** and **Mahboubeh Pishnamazi** gathered experimental adsorption data by flame atomic absorption spectroscopy and contributed to the final manuscript. **Azam Marjani** gathered experimental adsorption data by flame atomic absorption spectroscopy, contributed to the final manuscript, and also provided chemicals and laboratory equipment. **Saeed Shirazian** supervised the findings of this work, supervised the project, provided chemicals and laboratory equipment, and edited the paper. All authors verified the analytical methods.

Competing interests

The authors declare no competing interests.

References

1. Yang, S., Wu, Y., Wu, Y. & Zhu, L. Optimizing decolorization of Acid Fuchsin and Acid

Orange II solution by MnO2 loaded MCM-41. *J. Taiwan Inst. Chem. Eng.* **50**, 205-214 (2015).

2. Forgacs, E., Cserháti, T. & Oros, G. Removal of synthetic dyes from wastewaters: A review. *Environ. Int.* **30**, 953-971 (2004).

3. Padhi, B. Pollution due to synthetic dyes toxicity & carcinogenicity studies and remediation. *Int. J. Environ. Sci.* **3**, 940-955 (2012).

4. Guo, Y. J., Pan, J. H. & Jing, W. J. Determination of Orange II and the supramolecular system of Orange II with cyclodextrins by polarography. *Dye. Pigment.* **63**, 65-70 (2004).

5. Renita, A. A., Kumar, P. S. & Jabasingh, S. A. Redemption of acid fuchsin dye from wastewater using de-oiled biomass: Kinetics and isotherm analysis. *Bioresour. Technol. Reports* **7**, 100300 (2019).

6. Soltani, R., Marjani, A. & Shirazian, S. A hierarchical LDH/MOF nanocomposite: Single, simultaneous and consecutive adsorption of a reactive dye and Cr(vi). *Dalt. Trans.* **49**, 5323–5335 (2020).

7. Soltani, R., Marjani, A., Hosseini, M. & Shirazian, S. Mesostructured Hollow Siliceous Spheres for Adsorption of Dyes. *Chem. Eng. Technol.* **43**, 392–402 (2020).

8. Soltani, R., Marjani, A., Moguei, M. R. S., Rostami, B. & Shirazian, S. Novel diamino-functionalized fibrous silica submicro-spheres with a bimodal-micro-mesoporous network: Ultrasonic-assisted fabrication, characterization, and their application for superior uptake of Congo red. *J. Mol. Liq.* **294**, 111617 (2019).

9. Yagub, M. T., Sen, T. K., Afroze, S. & Ang, H. M. Dye and its removal from aqueous solution by adsorption: A review. *Adv. Colloid Interface Sci.* **209**, 172–184 (2014).

10. Soltani, R., Marjani, A., Hosseini, M. & Shirazian, S. Meso-architectured siliceous hollow quasi-capsule. *J. Colloid Interface Sci.* **570**, 390–401 (2020).

11. Adeyemo, A. A., Adeoye, I. O. & Bello, O. S. Metal organic frameworks as adsorbents for dye adsorption: Overview, prospects and future challenges. *Toxicol. Environ. Chem.* **94**, 1846-1863 (2012).

12. Li, J., Zhou, X., Wang, J. & Li, X. Two-Dimensional Covalent Organic Frameworks (COFs) for Membrane Separation: A Mini Review. *Ind. Eng. Chem. Res.* **58**, 15394-15406 (2019).

13. Soltani, R., Shahvar, A., Gordan, H., Dinari, M. & Saraji, M. Covalent triazine framework-decorated phenyl-functionalised SBA-15: Its synthesis and application as a novel nanoporous adsorbent. *New J. Chem.* **43**, 13058-13067 (2019).

14. Thakur, K. & Kandasubramanian, B. Graphene and Graphene Oxide-Based Composites for Removal of Organic Pollutants: A Review. *J. Chem. Eng. Data*. **64**, 833-867 (2019).

15. Khurana, I., Saxena, A., Bharti, Khurana, J. M. & Rai, P. K. Removal of Dyes Using Graphene-Based Composites: a Review. *Water. Air. Soil Pollut.* **228**, 180 (2017).

16. Huang, C. H., Chang, K. P., Ou, H. De, Chiang, Y. C. & Wang, C. F. Adsorption of cationic dyes onto mesoporous silica. *Microporous Mesoporous Mater.* **141**, 102-109 (2011).

17. Cashin, V. B., Eldridge, D. S., Yu, A. & Zhao, D. Surface functionalization and manipulation of mesoporous silica adsorbents for improved removal of pollutants: A review. *Environmental Science: Water Res. Technol.* **4,** 110-128 (2018).

18. Da'na, E. Adsorption of heavy metals on functionalized-mesoporous silica: A review. *Microporous Mesoporous Mater*. **247**, 145-157 (2017).

19. Polshettiwar, V., Cha, D., Zhang, X. & Basset, J. M. High-surface-area silica nanospheres (KCC-1) with a fibrous morphology. *Angew. Chemie - Int. Ed.* **49**, 9652-9656 (2010).

20. Bayal, N., Singh, B., Singh, R. & Polshettiwar, V. Size and Fiber Density Controlled Synthesis of Fibrous Nanosilica Spheres (KCC-1). *Sci. Rep.* **6**, 24888 (2016).

21. Sun, Z. *et al.* Multifunctional fibrous silica composite with high optical sensing performance and effective removal ability toward Hg^{2+} ions. *J. Mater. Chem. B* **3**, 3201-3210 (2015).

22. Zarei, F., Marjani, A. & Soltani, R. Novel and green nanocomposite-based adsorbents from functionalised mesoporous KCC-1 and chitosan-oleic acid for adsorption of Pb(II). *Eur. Polym. J.* **119**, 400–409 (2019).

23. Soltani, R., Marjani, A., Hosseini, M. & Shirazian, S. Synthesis and characterization of novel N-methylimidazolium-functionalized KCC-1: A highly efficient anion exchanger of

hexavalent chromium. *Chemosphere* **239**, 124735 (2020).

24. Yu, K., Zhang, X., Tong, H., Yan, X. & Liu, S. Synthesis of fibrous monodisperse core-shell Fe3O 4/SiO2/KCC-1. *Mater. Lett.* **106**, 151-154 (2013).

25. Soltani, R., Marjani, A. & Shirazian, S. Facile one-pot synthesis of thiol-functionalized mesoporous silica submicrospheres for Tl(I) adsorption: Isotherm, kinetic and thermodynamic studies. *J. Hazard. Mater.* **371**, 146–155 (2019).

26. Fan, H. T. *et al.* Removal of cadmium(II) and lead(II) from aqueous solution using sulfur-functionalized silica prepared by hydrothermal-assisted grafting method. *Chem. Eng. J.* **198**–**199**, 355-363 (2012).

27. Li, Y. *et al.* Small size mesoporous organosilica nanorods with different aspect ratios: Synthesis and cellular uptake. *J. Colloid Interface Sci.* **512**, 134-140 (2018).

28. Dhiman, M., Chalke, B. & Polshettiwar, V. Organosilane oxidation with a half million turnover number using fibrous nanosilica supported ultrasmall nanoparticles and pseudo-single atoms of gold. *J. Mater. Chem. A* **5**, 1935-1940 (2017).

29. Wu, Y., Zhang, M., Zhao, H., Yang, S. & Arkin, A. Functionalized mesoporous silica material and anionic dye adsorption: MCM-41 incorporated with amine groups for competitive adsorption of Acid Fuchsine and Acid Orange II. *RSC Adv.* **4**, 61256-61267 (2014).

30. Wang, Q. *et al.* Rapid simultaneous adsorption and SERS detection of acid orange II using versatile gold nanoparticles decorated NH2-MIL-101(Cr). *Anal. Chim. Acta* **1129**, 126-135 (2020).

31. Yang, Z., Zhu, L. & Chen, L. Selective adsorption and separation of dyes from aqueous solution by core-shell structured NH_2-functionalized UiO-66 magnetic composites. *J. Colloid Interface Sci.* **539**, 76-86 (2019).

32. Gong, N., Liu, Y. & Huang, R. Simultaneous adsorption of Cu^{2+} and Acid fuchsin (AF) from aqueous solutions by CMC/bentonite composite. *Int. J. Biol. Macromol.* **115**, 580-589 (2018).

33. Jin, X., Yu, B., Chen, Z., Arocena, J. M. & Thring, R. W. Adsorption of Orange II dye in aqueous solution onto surfactant-coated zeolite: Characterization, kinetic and thermodynamic studies. *J. Colloid Interface Sci.* **435**, 15-20 (2014).

34. Zhou, Y., Hu, X., Zhang, M., Zhuo, X. & Niu, J. Preparation and characterization of modified cellulose for adsorption of Cd(II), Hg(II), and acid fuchsin from aqueous solutions. *Ind. Eng. Chem. Res.* **52**, 876-884 (2013).

Figures

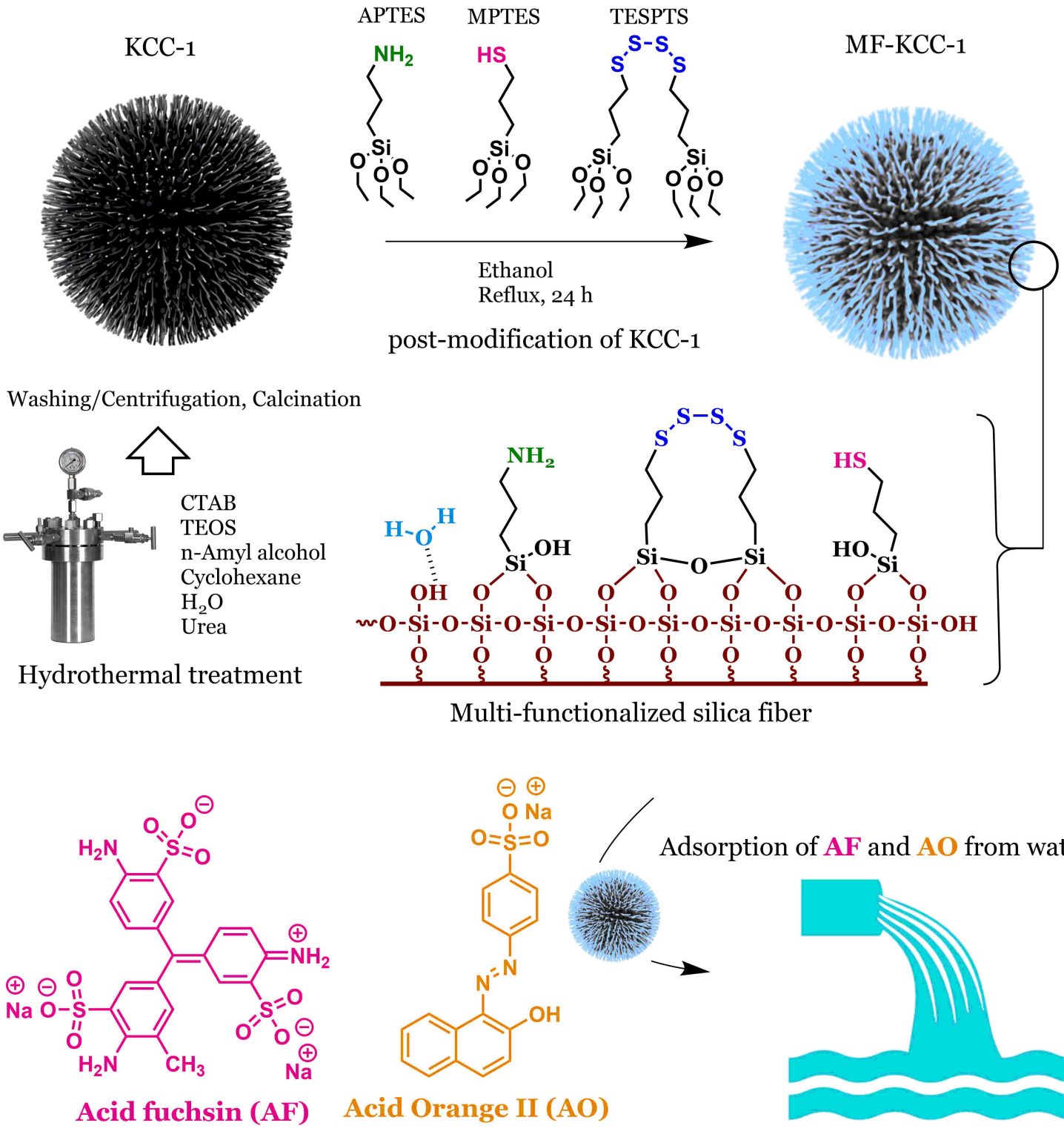

Figure 1

The overall process of synthesizing KCC-1 and MF-KCC-1 and molecular structure of AF and AO dyes.

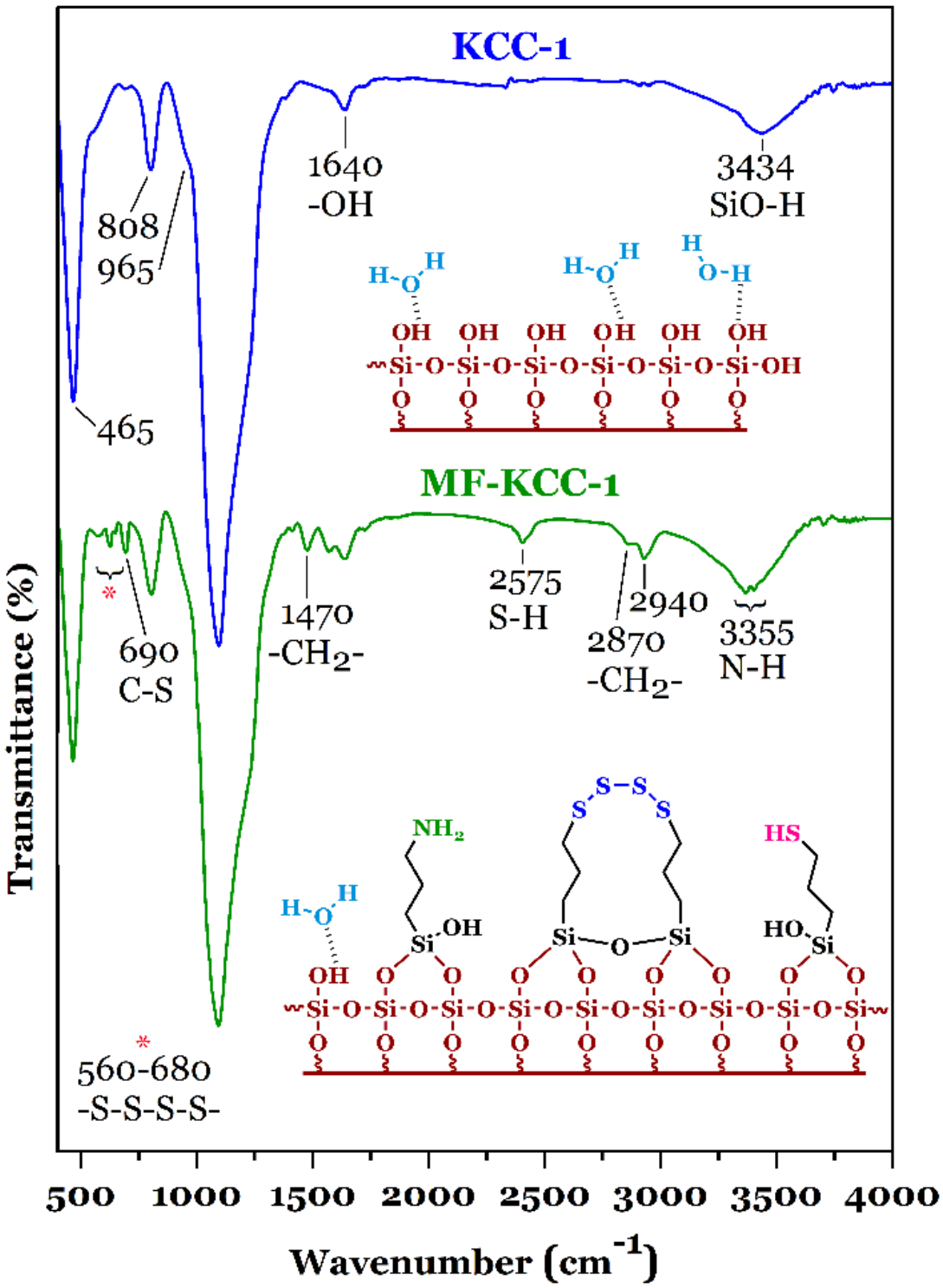

Figure 2

FTIR spectra of the samples.

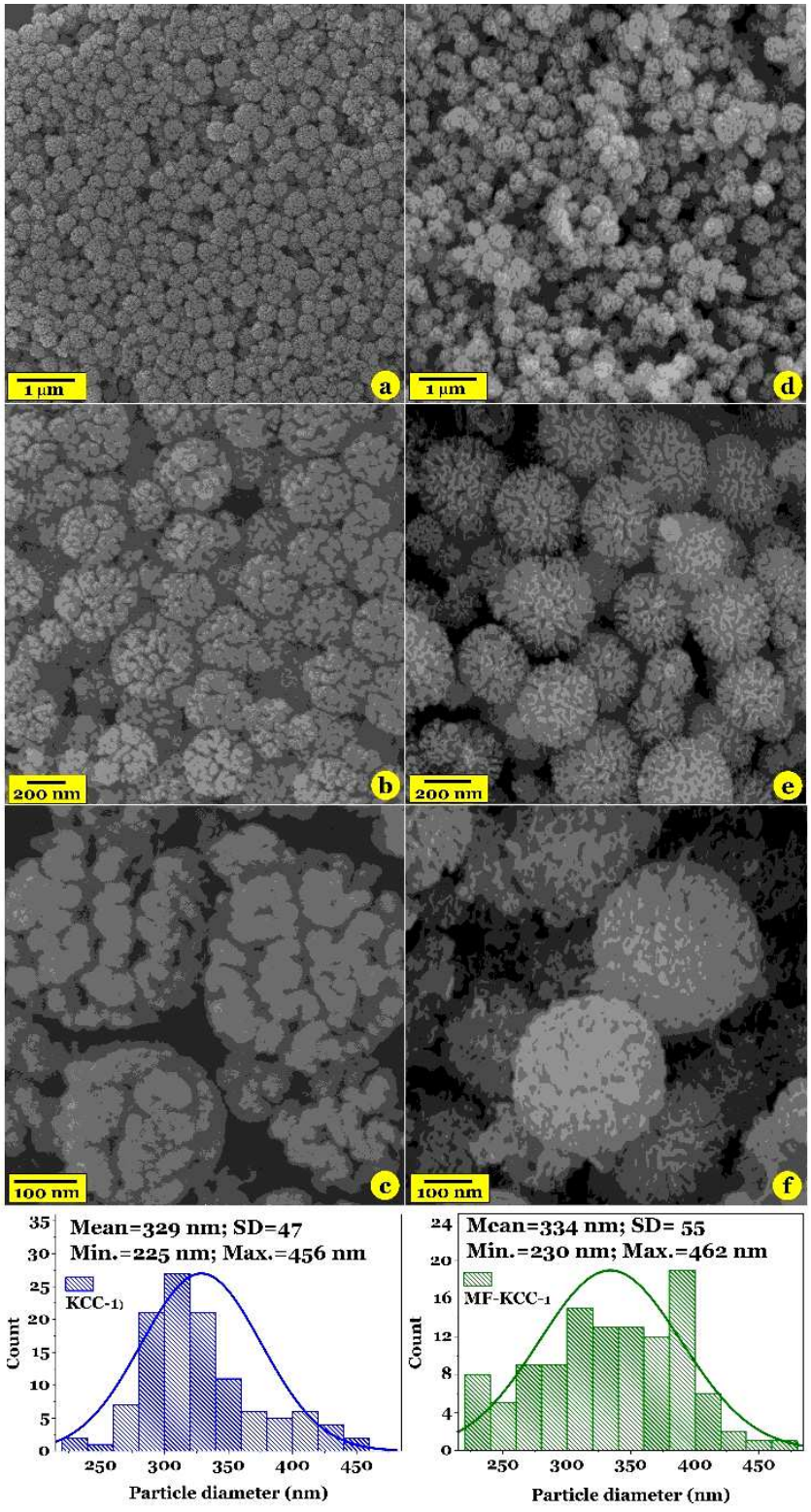

Figure 3

FESEM images of pure KCC-1 (a-c) and MF-KCC-1 (d-f) and corresponding particle size histograms.

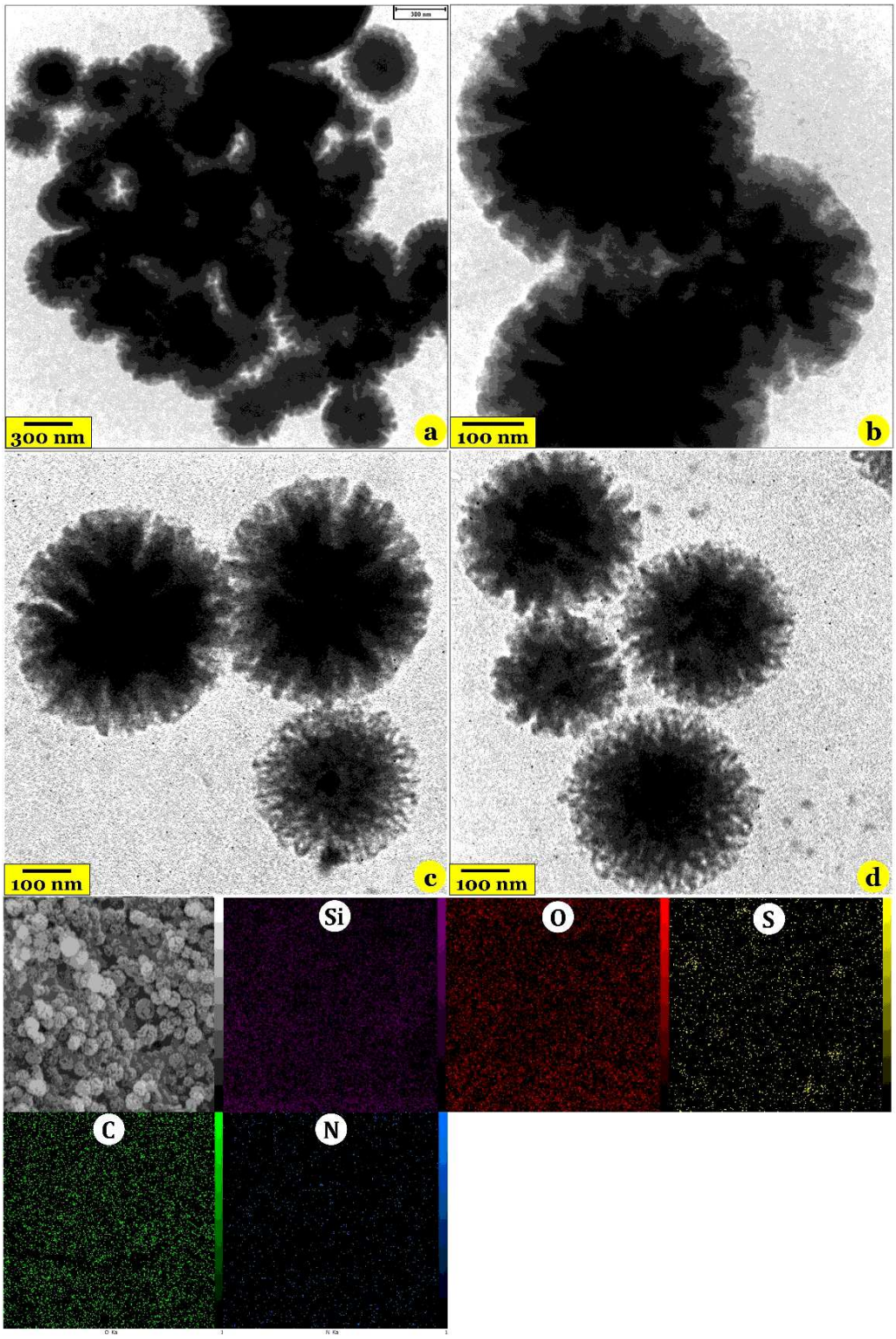

Figure 4

TEM images of the pure KCC-1 (a and b) and MF-KCC-1 (c and d) and EDX dot elemental mapping images of the MF-KCC-1 (the third and fourth rows).

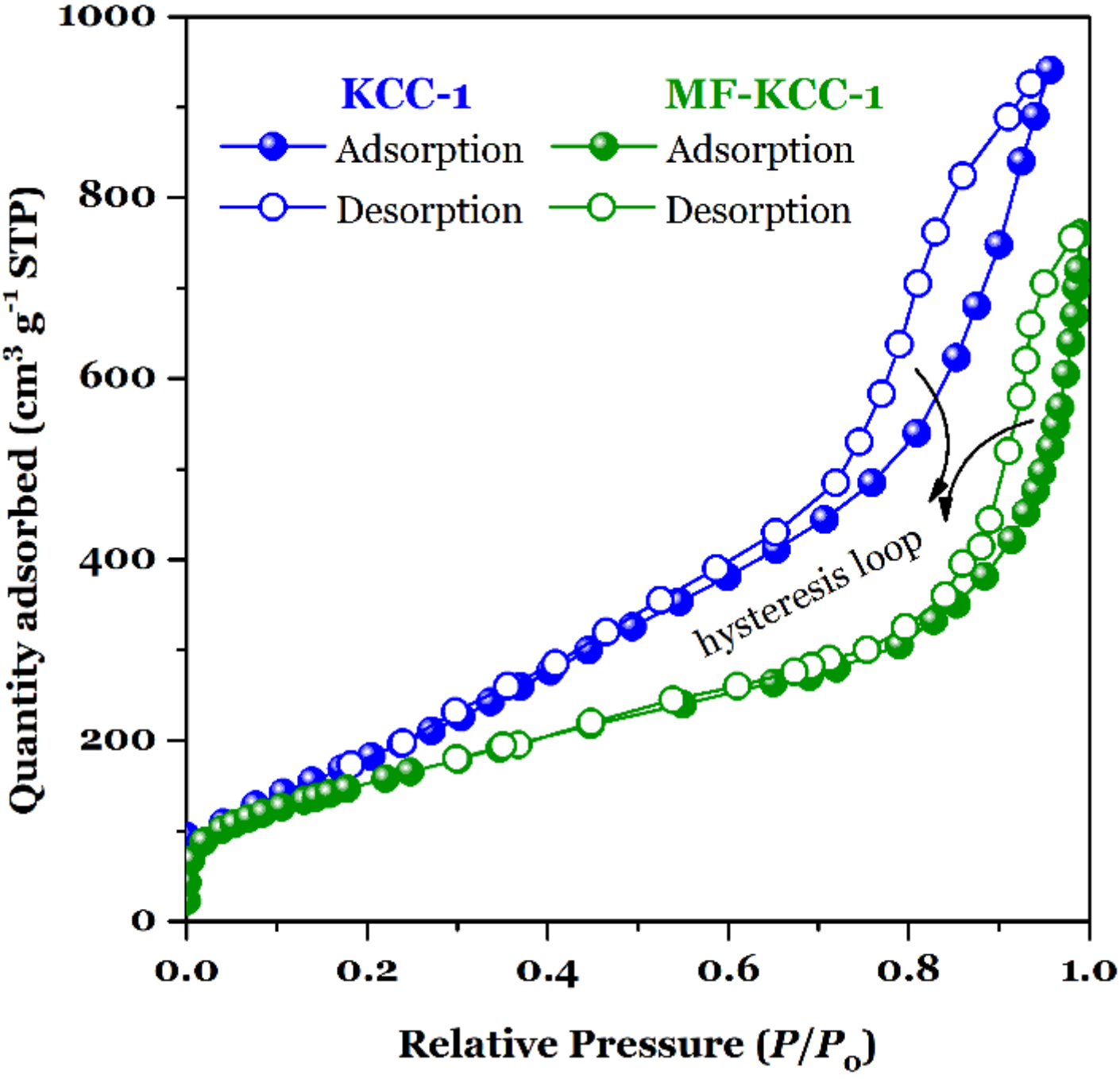

Figure 5

The N2 adsorption-desorption isotherms of KCC-1 and MF-KCC-1.

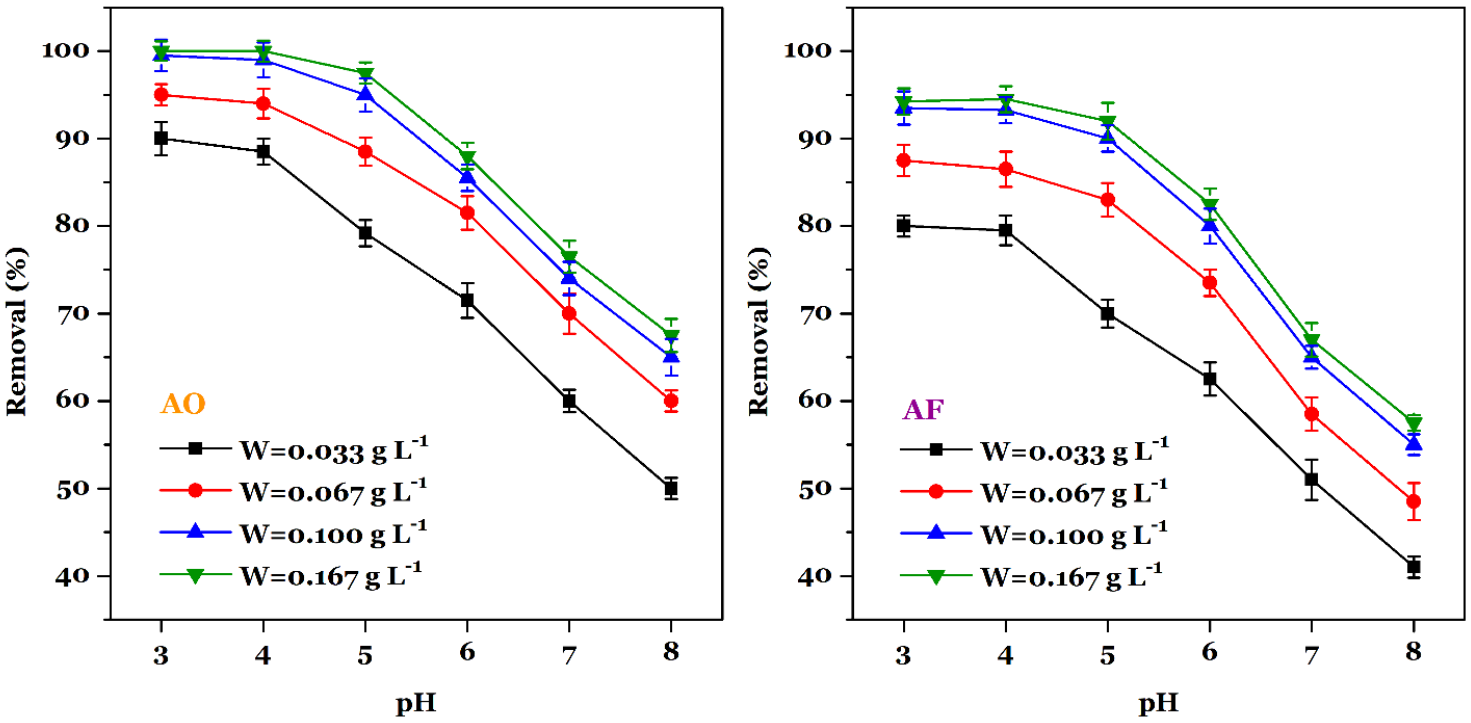

Figure 6

The effect of pH and adsorbent dosage on the removal percentage of AF (left) and AO (right) dyes (Ci=10 mg L−1, t=120 min, T=25 ℃, shaking speed =180 rpm).

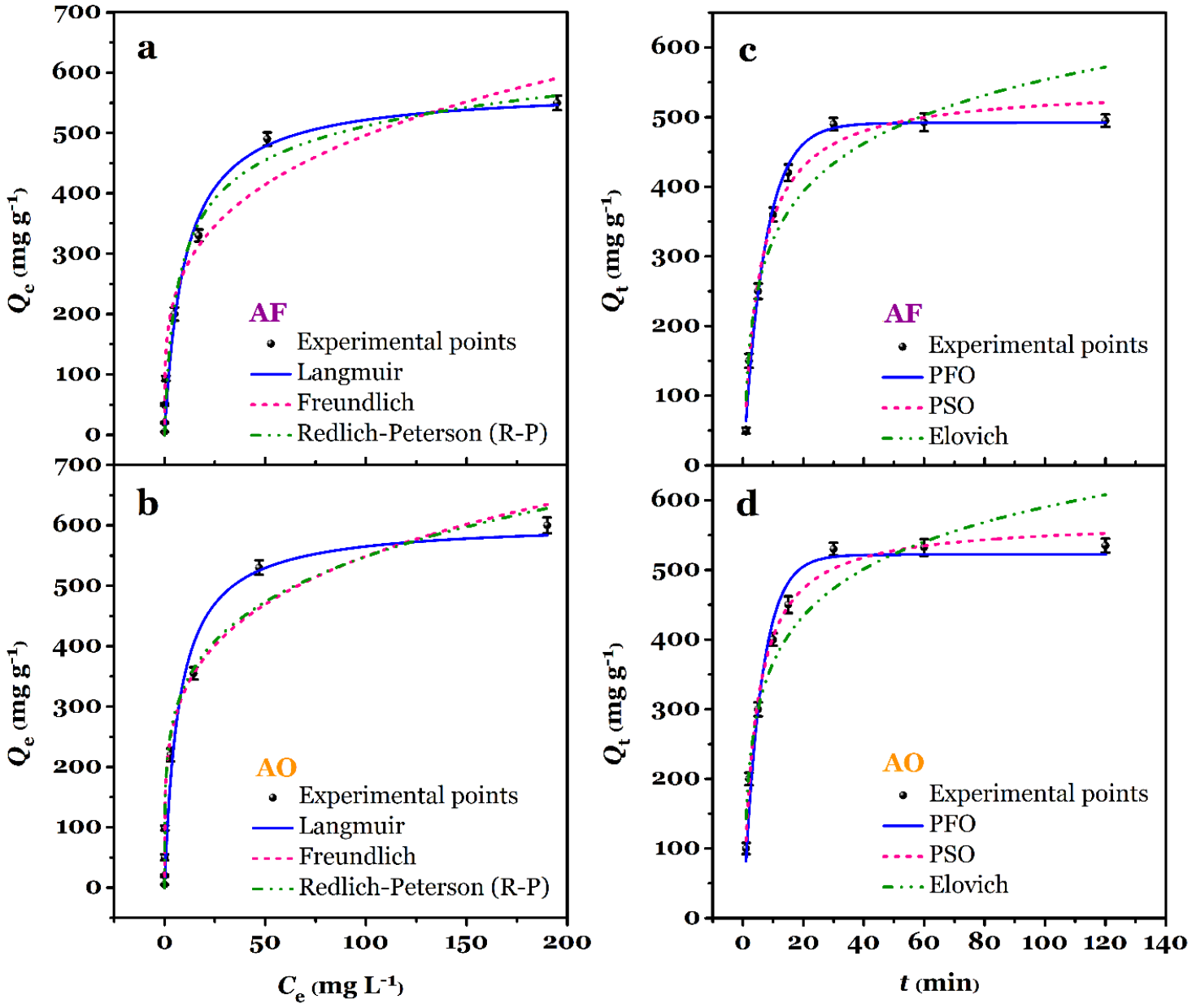

Figure 7

The effect of initial dye concentration on the adsorption capacity of AF (a) and AO (b) dyes and corresponding isotherm curves (pH=3.0, W= 0.100 g L−1, Ci=0.5-250 mg L−1, t=120 min, T=25 ℃, shaking speed=180 rpm). The effect of time on the adsorption capacity of AF (a) and AO (b) dyes and corresponding kinetic curves (pH=3.0, W= 0.100 g L−1, Ci=100 mg L−1, t=1-120 min, T=25 ℃, shaking speed=180 rpm).